Check for updates

Research Article
Open Access

MJ Cell Press

MJ Engineering Sciences

Available at: https://mjcellpress.com/article/mjes11/

MJ Engineering Sciences

Influence of Varying Focal Length on the Performance of a Solar Cooker

Wandji Kepdjouo Nathanaël[1*], Ekani Roger Yannick[2,3], Tetang Fokone Abraham[1], Djiako Thomas[4], Edoun Marcel[1].

[1] Department of Energy Engineering, Electronics and Automation, ENSAI, University of Ngaoundere, Ngaoundere, Cameroon.

[2] Energy Laboratory, National Higher Polytechnic School of Douala, University of Douala, BP 2701, Douala, Cameroon.

[3] Experimentation and Production Centre, National Higher School of Maritime and Oceanic Sciences and Technologies, University of Ebolowa, BP 292, Kribi, Cameroon.

[4] University Institute of the Gulf of Guinea, Douala, Cameroon.

[*]Corresponding author: nathanwandji00@gmail.com

Key words

Solar cooker,
Focal length,
Parabolic concentrator,
Simulation,
Steady state,
Factor of non-uniformity.

.

Abstract

Access to clean and sustainable cooking energy remains a major challenge in many developing regions, where reliance on biomass fuels contributes to deforestation and adverse health effects. Parabolic solar cookers offer a promising solution due to their high-temperature potential; however, their performance is often constrained by strong thermal non-uniformity resulting from excessive energy concentration at the geometric focus. This study investigates the influence of focal length variation on the thermal performance of a parabolic solar cooker under moderate solar irradiance conditions. A steady-state numerical analysis was carried out using a coupled Tonatiuh–ANSYS Fluent approach, based on the climatic conditions of Ngaoundéré (DNI = 450 $W \cdot m^{-2}$, ambient temperature = 298.15 K, wind speed = 1.5 $m \cdot s^{-1}$). Three focal configurations, including the geometric focus and two defocused positions, were examined. The results indicate that a slight downward displacement of the absorber improves both thermal performance and temperature uniformity. An optimal focal length of 0.70 m increases the maximum absorber and water temperatures by approximately 2.2 K and reduces the temperature non-uniformity factor by 23%. Controlled defocusing thus emerges as an effective strategy for enhancing the efficiency and practical reliability of parabolic solar cookers.

Received:01.07.2025 Accepted: 03.12.2025 Published online: 20.12.2025

How to cite this article: Wandji Kepdjouo, N., Ekani, R. Y., Tetang Fokone, A., Djiako, T., & Edoun, M. (2025). *Influence of varying focal length on the performance of a solar cooker*. MJ Engineering Sciences. *1*(2), 160–173. https://doi.org/10.63156/mjes11

1. Introduction

Access to clean and sustainable cooking energy remains a major challenge in many developing countries, where heavy reliance on biomass fuels exacerbates deforestation and leads to significant health problems associated with household smoke (BEHEKE, 2021; IEA, 2022). In response to these challenges, solar cooking technologies have emerged as a promising alternative, as they exploit an abundant, renewable, and freely available energy resource (Dontio, Guemene, Efa, & Simo, 2010; Mahmut & Saffa, 2015).

Among solar cooking devices, the literature generally distinguishes between calendar (or box-type) cookers (Coccia, Aquilanti, Tomassetti, Comodi, & Nicola, 2020; Schwarzer & Silva, 2008; Telkes, 1959; Zafar, Khan, Badar, Tariq, & Butt, 2018) and concentrating cookers (Ahmed et al., 2020; Franco, Cadena, & Saravia, 2004; Herez, Ramadan, & Khaled, 2018). Calendar cookers are characterized by relatively low operating temperatures, typically in the range of 120–130 °C, which results in long cooking times and limits their practical applicability (Harmim, Belhamel, & Bouhadda, 2010). In contrast, parabolic solar cookers are capable of concentrating solar radiation to rapidly achieve high temperatures, often reaching up to 300 °C, thereby significantly accelerating the cooking process and making them attractive for everyday use (Cuce, Cuce, & Bali, 2016; Schwarzer & Silva, 2008).

Despite their high thermal potential, parabolic cookers suffer from an inherent limitation related to the strong concentration of heat flux at a highly localized focal point, commonly referred to as a hot spot (Khalifa & Al-Mutawa, 1993; Othman, 2006). Conventionally, the absorber is positioned exactly at the geometric focus of the reflector (f = 0.78 m in the present case). However, this configuration often leads to severe thermal non-uniformity across the pot surface, resulting in localized overheating, degradation of surface coatings, and increased heat losses (El-Sebaii & Al-Ghamdi, 2012). The existing research gap lies in the hypothesis that a slight displacement of the absorber, known as defocusing, could effectively spread the focal region and improve heat distribution (Kihwele, Njau, & Mushi, 2020). Consequently, iso-intensity configurations have been identified as a promising approach for simultaneously enhancing heating quality and overall thermal efficiency (Kalogirou, 2004).

In this context, the present study aims to analyze the influence of focal length variation (f) on the performance of a parabolic solar cooker operating under the moderate climatic conditions of Ngaoundéré (DNI = 450 $W \cdot m^{-2}$). The specific objectives are: (i) to determine the optimal focal length that maximizes thermal performance, (ii) to quantify the improvement in maximum temperature (T_max) at both the absorber and the water relative to the geometric focus, and (iii) to evaluate the reduction in thermal non-uniformity (ΔT) across the absorber surface. A steady-state analysis of T_max and ΔT is adopted as a relevant indicator of the potential for accelerating cooking time, thereby justifying the use of a coupled Tonatiuh/ANSYS Fluent numerical approach, which has been successfully applied in several advanced studies on solar concentrating systems (Fernández-Reche, Sansom, & Martínez, 2019; Reda, Andreas, & Sengupta, 2014).

2. Physical model

The physical configuration of the parabolic solar cooker investigated in this study is illustrated in Figure 1. The analysis focuses on the influence of the focal length on the thermal performance of the system by considering several focal positions while keeping the overall geometry of the cooker unchanged.

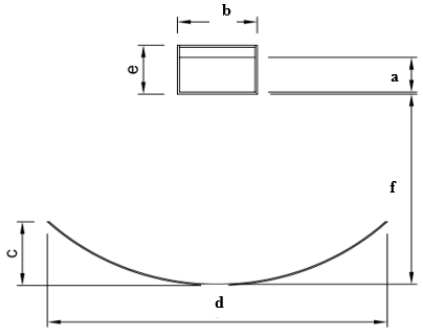

Figure 1. Physical model of the studied parabolic solar cooker.

Three focal length values were examined in order to assess the effect of controlled defocusing. These values, including the geometric focal length and two shifted positions, are summarized in Table 1.

Table 1. Investigated focal length values.

$f_{1\,(m)}$	$f_{(m)}$	$f_{2(m)}$
0.7	0.78	0.86

2.1 Reflector

The parabolic reflector constitutes the primary concentrating element of the solar cooker. Its geometric characteristics are reported in **Table 2**. The reflector has an aperture diameter of 1.81 m and a focal length of 0.78 m, corresponding to the geometric focus. The resulting catchment area is 2.57 m², with an opening angle of 59.7°, ensuring effective solar radiation interception.

Table 2. Physical characteristics of the reflector.

Sizes	Values
Diameter (m)	1.81
Size (m)	0.26
Focal lengths (m)	0.78
Catchment area (m^2)	2.57
Opening angle (ψ)	59.7°

2.2 Absorber

The absorber used in this study represents a conventional cooking pot designed for everyday domestic use. Its geometric characteristics are given in Table 3. The absorber has a diameter of 0.30 m and a height of 0.20 m, resulting in an effective catchment area of 0.2826 m². This geometry allows direct interaction with the concentrated solar flux delivered by the parabolic reflector.

Table 3. Physical characteristics of the absorber.

Sizes	Values
Diameter (m)	0.3
Height (m)	0.2
Catchment area (m^2)	0.2826

2.3 Load

The thermal load considered in this study is running water contained within the absorber. Water was selected due to its relevance to cooking applications and its well-known thermophysical properties, which facilitate reliable numerical modeling of heat transfer processes.

2.4 Thermophysical properties

The thermophysical properties of the materials composing the reflector, absorber, and load are summarized in Table 4. These properties were assumed constant over the investigated temperature range and were used as input parameters in the numerical simulations.

Table 4. Thermophysical properties of the components of the solar cooker.

Component	Materials	Density $\rho(kg.m^{-3})$	Specific heat C_p $(J.kg^{-1}.K^{-1})$	Thermal conductivity $\lambda\,(W.m^{-1}.K^{-1})$	Absorptivity α	Emissivity ε	Specular Reflectance ρ_{spec}
Reflector	Aluminum	2700	900	237	0.05	0.05	0.90

Absorb	Black painted aluminum	2700	900	237	0.90	0.90	-
Charge	Water	1000	4180	0.61	-	-	-

3. Simulation method

3.1 Radiation modeling using Tonatiuh

The modeling of the concentrated solar heat flux was carried out using the Tonatiuh ray-tracing code, which is widely employed for the optical analysis of solar concentrating systems. Tonatiuh allows accurate computation of the spatial distribution of the incident solar flux on the absorber surface, which is subsequently imported into ANSYS Fluent for thermal analysis.

To ensure the reliability and accuracy of the generated flux maps, the following optical parameters were adopted. The solar source was represented using a Gaussian cone model, with the half-angle of the sun fixed at 4.65 mrad, corresponding to standard solar angular divergence. A total of 100 rays were launched, which was found sufficient to ensure statistical convergence of the flux distribution over the relatively small absorber surface. The overall optical error, including profile and tracking inaccuracies, was set to 1.0 mrad, representative of the optical quality of a low-cost parabolic reflector. The specular reflectance of the reflector was fixed at 0.90, in accordance with the material properties reported in Table 4, and the reflectance was assumed constant over the effective solar spectrum. Tonatiuh computes the incident radiative power directly without requiring manual specification of view factors. The resulting spatial heat flux distribution was then exported and used as an input boundary condition in the CFD simulations performed with ANSYS Fluent.

3.2 CFD modeling and heat transfer

The thermal behavior of the solar cooker was investigated using ANSYS Fluent, where the radiative heat flux obtained from Tonatiuh was coupled with fluid flow and heat transfer calculations. All simulations were conducted under steady-state operating conditions. Heat transfer mechanisms considered in the model include forced convection induced by wind, natural convection within the water load and the surrounding air, and thermal radiation exchanges between the absorber, reflector, and the environment. The flow of air and water was modeled using the standard k–ε turbulence model, combined with the SIMPLE algorithm, which is well suited for predicting convective heat transfer and temperature gradients in similar systems.

Radiative heat exchange with the surroundings was considered through surface emissivity. The absorber emissivity was fixed at $\varepsilon = 0.90$, and radiative transfer was modeled using the Discrete Ordinates (DO) model or an equivalent surface-to-surface radiation formulation. The sky was assumed to be at ambient temperature ($T_{amβ} = 298.15$ K).

3.3 Boundary conditions and meteorological inputs

The boundary conditions applied to the external surfaces of the computational domain, including the parabolic reflector and the cooking pot, were defined based on local meteorological data. The Direct Normal Irradiance (DNI) was fixed at 450 $W \cdot m^{-2}$, corresponding to moderate solar conditions in Ngaoundere. Wind effects were introduced using a uniform inlet velocity of $U\_wind = 1.5\ m \cdot s^{-1}$.

To simplify the estimation of forced convection on exposed external surfaces, the wind convection coefficient (h_wind) was calculated using a standard empirical correlation:

$$h_{\text{wind}} = 5.7 + 3.8\,U_{\text{wind}}$$

which yields $h\_wind = 11.4\ W \cdot m^{-2} \cdot K^{-1}$ for the selected wind speed.

3.4 Convergence criteria

The convergence of the numerical solution was ensured by imposing a strict residual threshold of 10^{-6} for all governing equations, including continuity, momentum, and energy. This criterion guarantees the stability and accuracy of the stationary solution.

3.5 Numerical solution procedure

The numerical simulations were based on the **finite volume method**, which ensures conservation of mass, momentum, and energy across each control volume within the computational domain. The domain was discretized into a finite number of control volumes centered on computational nodes. Using appropriate discretization schemes, the governing equations were integrated over each control volume, and nonlinear terms were linearized to facilitate convergence.

The overall numerical workflow implemented in ANSYS Fluent is summarized schematically below.

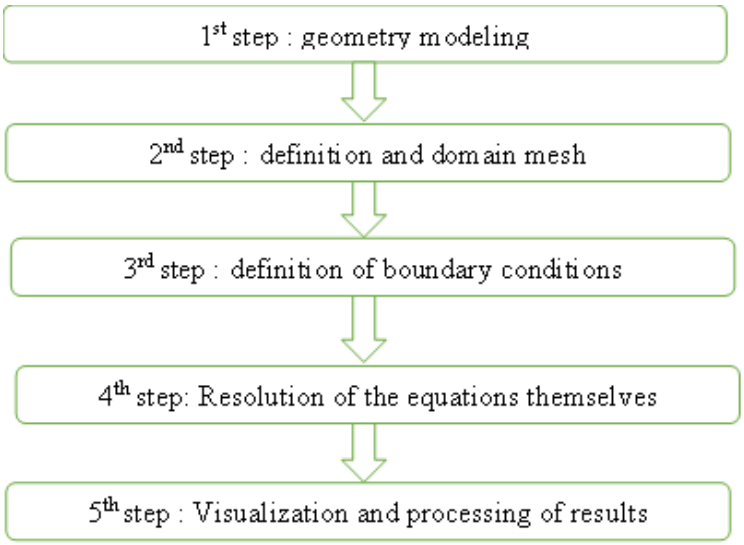

Figure 2. Simulation approach with ANSYS Fluent.

The chronological sequence of the numerical calculation, including initialization, iterative resolution, convergence monitoring, and validation, is illustrated in the following flowchart.

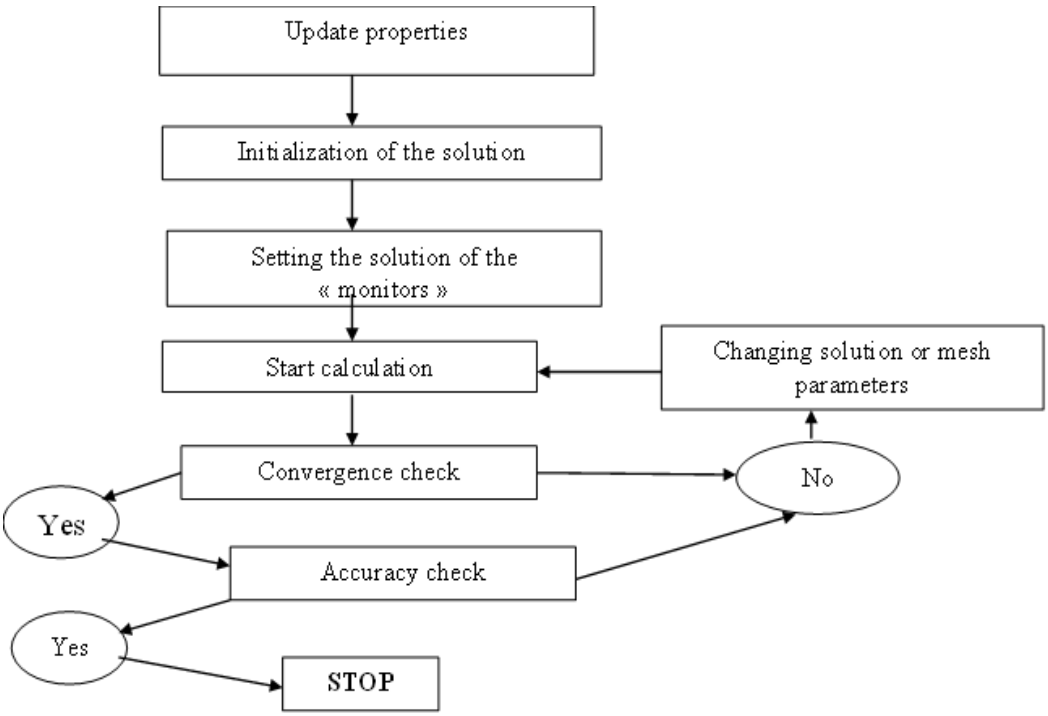

Figure 3. Chronology of the numerical calculation.

3.6 Modeling of solar irradiation and ambient temperature

The temporal variation of ambient temperature and solar irradiation was modeled using the empirical relations proposed by Oudjedi et al. (2008). The ambient temperature is expressed as:

$$T_{amb} = T_1 + T_2 \cos\left[\frac{\pi}{12}(14 - TSV)\right] + 273.15 \quad (1)$$

With

$$T_1 = \frac{T_{amb\text{-}max} + T_{amb\text{-}min}}{2} \quad (2)$$

$$T_2 = \frac{T_{amb\text{-}max} - T_{amb\text{-}min}}{2} \quad (3)$$

3.7 Modeling of parabolic geometry

A parabola is defined as the locus of points equidistant from a fixed point (the focus) and a fixed line (the directrix), as illustrated below.

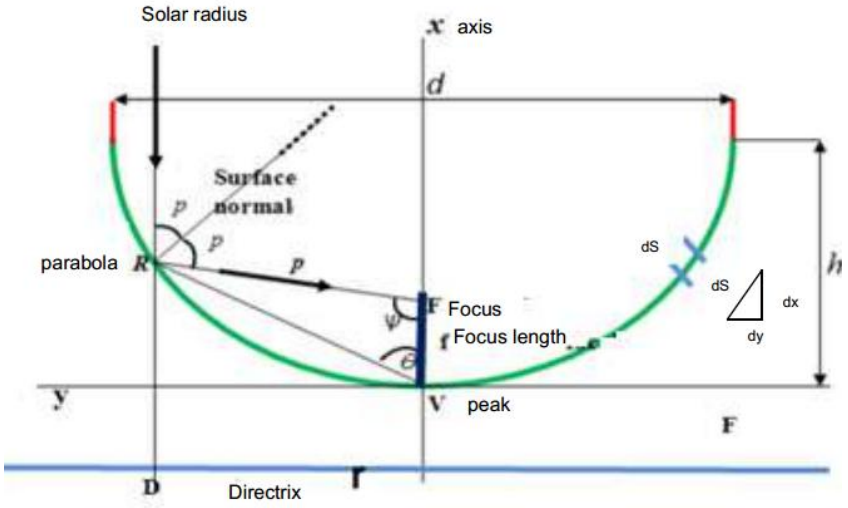

Figure 4. Parabolic geometry.

When the origin is placed at the vertex (V) and the x-axis aligned with the axis of symmetry, the equation of the parabola is given by (Kurzweg & Benson, 1982):

$$y^2 = 4fx \quad (4)$$

If the origin is shifted toward the focus (F), the equation becomes:

$$y^2 = 4f(x + f) \quad (5)$$

The parabolic profile can also be expressed as a function of the focal length f and the opening angle ψ

$$P = \frac{2f}{1 + \cos\psi} \quad (6)$$

3.8 Geometric characteristics of the parabola

For a parabolic reflector with aperture diameter d and focal length f, the height h of the parabola is given by (Srinivasan & Kulkarni, 1978):

$$h = \frac{d^2}{2f} \tag{7}$$

The arc length of the parabolic dish is expressed as (Braun & Mitchell, 1983):

$$S = \frac{d}{2}\sqrt{\left(\frac{4h}{d}\right)^2 + 2} + 2f \ln\left[\frac{4h}{d} + \sqrt{\left(\frac{4h}{d}\right)^2 + 1}\right] \tag{8}$$

The surface area is given by: $A_x = \frac{2}{3}dh$ (9)

The opening angle of the parabola is defined by:

$$\psi = 2P \tag{10}$$

$$\tan\psi_p = \frac{(f/d)}{2(f/d)^2 - 1/8} \tag{11}$$

4. Results and discussion

4.1 Coupling between the cooker and the water load

The numerical mesh used for the parabolic cooker and the water load is illustrated below. This mesh was generated to accurately capture heat transfer and fluid flow phenomena within the system.

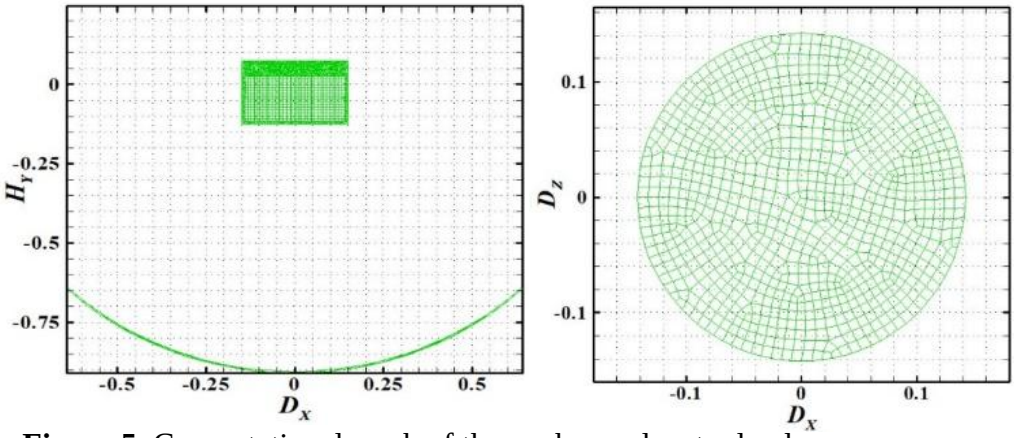

Figure 5. Computational mesh of the cooker and water load.

The main characteristics of the computational grid are summarized in Table 5.

Table 5. Mesh characteristics of the cooker and water load.

	Reflector	Absorber	Charge (water)
Number of cells	1010	25940	14160
Number of faces	4090	60521	44521
Number of nodes	212	8651	15912

The adopted meshing strategy deliberately applies finer grids in regions where strong temperature gradients and heat flux variations are expected. In particular, the absorber and the water load were discretized with a higher mesh density than the reflector. This choice is technically justified by the fact that these zones govern the thermal performance indicators of interest, notably temperature distribution and convective heat transfer. The absorber exhibits the highest number of cells (25,940), confirming the need for high spatial resolution to accurately resolve heat transfer phenomena on this critical surface.

4.2 Profiles of incident and reflected solar rays

The optical behavior of the system was first analyzed through ray-tracing simulations. The profiles of incident and reflected solar rays obtained using the Tonatiuh code for different focal lengths are presented below (figure 6).

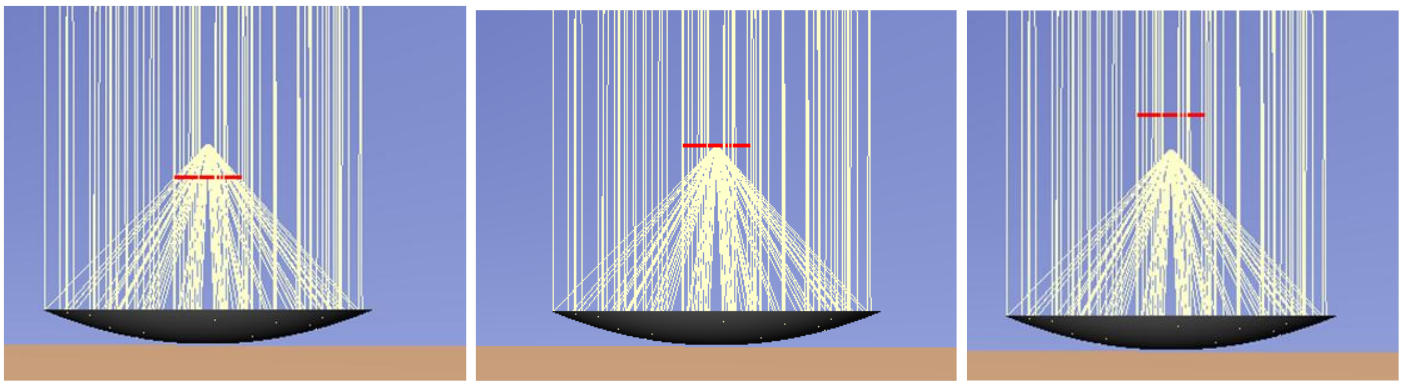

Figure 6. Profiles of incident and reflected solar rays: (a) f = 0.70 m; (b) f = 0.78 m; (c) f = 0.86 m.

These ray profiles clearly illustrate the effect of focal length variation on the spatial distribution of the concentrated solar radiation, highlighting changes in focal spot size and energy interception by the absorber.

4.3 Solar flux distribution on the absorber

The spatial distribution of the solar flux radiated onto the absorber surface is shown below (figure 7).

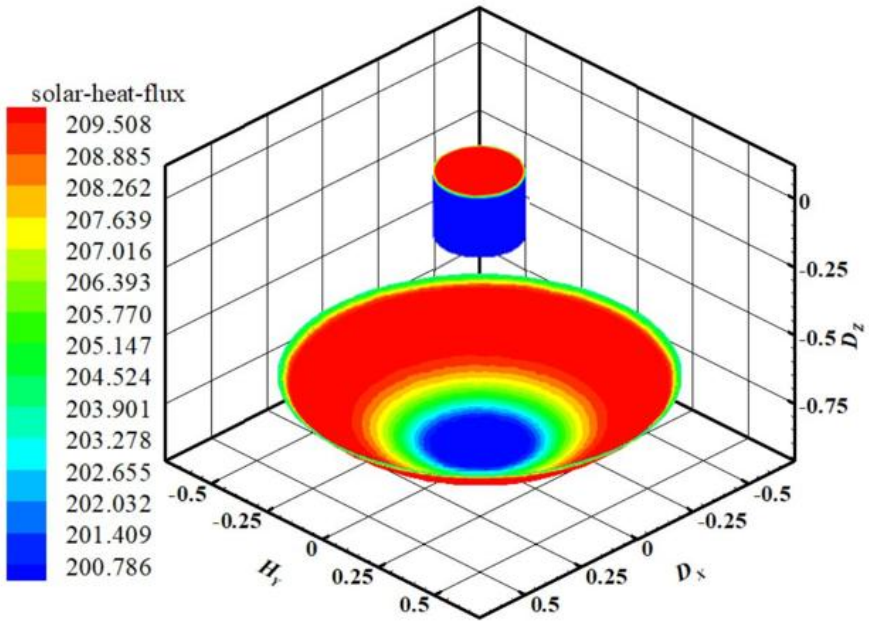

Figure 7. Solar flux field radiated onto the absorber.

The flux distribution over the parabolic dish is divided into five distinct zones, progressing from the center toward the edge. Due to the shadow cast by the absorber, the central region exhibits lower flux values. The minimum flux, observed in the central blue zone, is approximately 200.79 W·m^{-2}, while the maximum flux, located in the outer red region, reaches 209.51 W·m^{-2}. The average solar flux over the absorber surface is estimated at 205.89 W·m^{-2}, indicating a relatively uniform overall energy distribution despite local variations.

4.4 Absorber temperature field and non-uniformity analysis

The thermal response of the absorber was analyzed under the meteorological conditions of August 17, 2021, at 1:00 PM. The temperature fields obtained for the different focal length configurations are presented below.

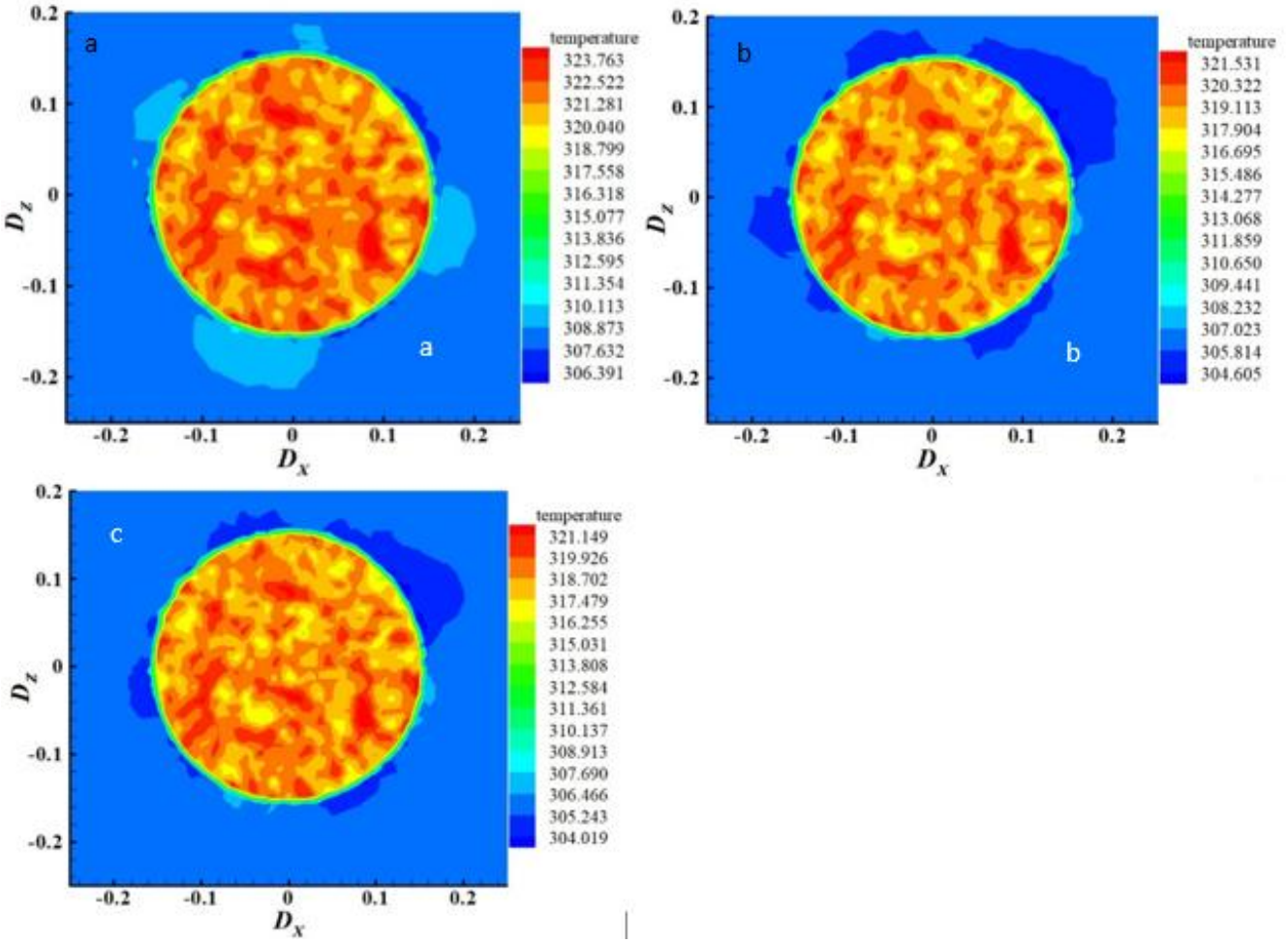

Figure 8. Absorber temperature fields: (a) f = 0.70 m; (b) f = 0.78 m; (c) f = 0.86 m.

A quantitative summary of the maximum and minimum absorber temperatures is provided in Table 6.

Table 6. Maximum and minimum absorber temperatures and temperature difference.

Focal length	T AbsMax (K)	T AbsMin (K)	ΔT_{Abs} (K)
Optimal (0.70m)	323,763	320,040	3.723
Geometric (0.78m)	321.531	316,696	4.835
Defocused (0.86m)	321.146	316,255	4.891

For all configurations, the absorber exhibits a relatively uniform temperature distribution, which can be attributed to combined effects of material properties, wind-induced convection, and the relative position of the pot with respect to the focal point. However, significant differences appear when comparing focal length configurations under identical simulation conditions.

At a focal length of 0.70 m, the absorber reaches a maximum temperature of 323.76 K and a minimum temperature of 320.04 K, corresponding to a temperature difference ΔT_Abs of 3.72 K. In contrast, the geometric focus

configuration (f = 0.78 m) yields a higher temperature non-uniformity (ΔT_Abs = 4.84 K), while the defocused case at f = 0.86 m shows a similar trend. The configuration at f = 0.70 m therefore appears optimal.

Although the absolute temperatures obtained in this steady-state study are lower than those reported experimentally by Soro et al. (2019), this discrepancy is explained by the moderate solar irradiance conditions considered (DNI = 450 $W \cdot m^{-2}$), corresponding to one of the least sunny periods in Ngaoundéré. Higher temperatures are expected under stronger solar conditions.

The 23% reduction in absorber temperature non-uniformity when moving from f = 0.78 m to f = 0.70 m demonstrates the benefit of controlled defocusing. While transient cooking tests would better represent real cooking times, steady-state indicators such as maximum temperature and thermal uniformity remain relevant predictors of cooking acceleration potential. The observed improvement is attributed to three main physical mechanisms: better adaptation between focal spot size and absorber diameter, reduction of localized overheating, and improved heat transfer toward the water load.

4.5 Temperature field of the water load and useful power

The temperature distribution within the water load was evaluated by extracting a cross-section of the pot located 15 cm above the bottom. The resulting temperature fields are shown below.

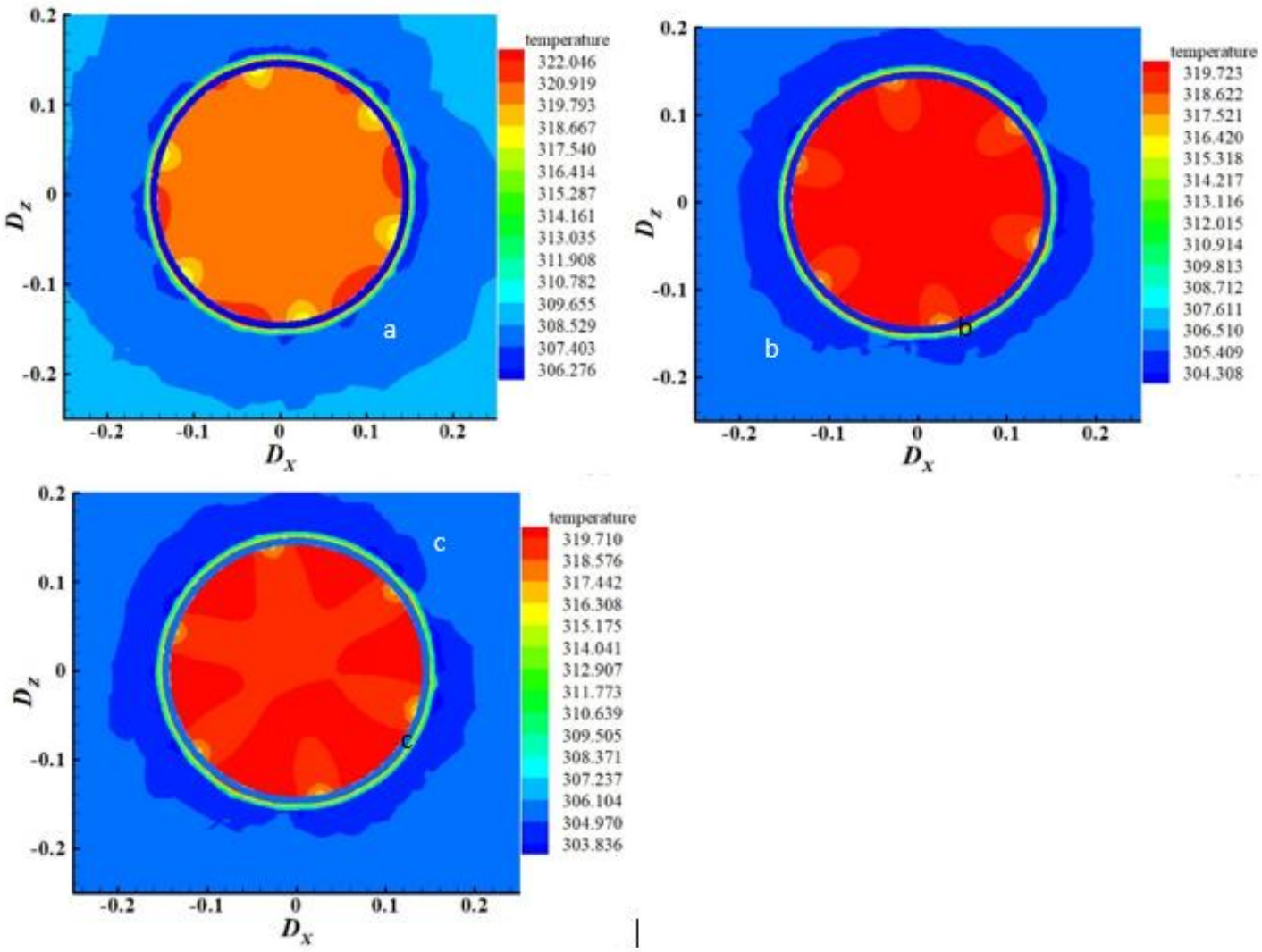

Figure 9. Water temperature fields: (a) f = 0.70 m; (b) f = 0.78 m; (c) f = 0.86 m.

The corresponding maximum and minimum water temperatures are summarized in Table 7.

Table 7. Maximum and minimum water temperatures and temperature difference.

Focal length	T EauMax (K)	T EauMin (K)	ΔT_{Eau} (K)
Optimal (0.70m)	322,046	318,667	3.379
Geometric (0.78m)	319.723	315.318	4.405
Defocused (0.86m)	319.710	316.308	3.402

Under steady-state conditions, the incident solar power on the reflector remains constant for all configurations:

$$Q_{\text{incident}} = DNI \times A_{\text{reflector}} = 450 \times 2.57 = 1156.5 \text{ W}$$

The maximum water temperature is therefore adopted as the main indicator of useful thermal power. The relative performance of each configuration is summarized in Table 8.

Table 8. Relative useful thermal performance.

Focal length (f)	T Max, Water (K)	$\Delta T = T_{Max,Eau} - T_{amb}$ (K)	Relative performance Q_{utile}
Optimal (0.70m)	322,046	23,896	+10.77%
Geometric (0.78m)	319.723	21.573	Référence (0%)
Defocused (0.86m)	319.710	21.560	-0.06%

The results confirm that the configuration with f = 0.70 m achieves the highest water temperature (322.05 K), corresponding to a relative performance increase of 10.77% compared to the geometric focus. The water temperature field is highly uniform, reflecting the homogeneous nature of the fluid. The temperature increase of approximately 2.3 K relative to the geometric focus demonstrates that controlled defocusing enhances useful heat transfer, leading to faster cooking. These results are consistent with experimental observations reported by Akoy and Ahmed (2015).

4.6 Mesh independence and validation

The final computational mesh retained in this study consists of approximately 41,000 cells. To verify mesh independence, simulations were performed using coarse, medium, and fine meshes. The results are summarized in Table 9.

Table 9. Mesh independence analysis.

Mesh	Number of cells	$T_{Max, Water}$ (K)	Relative variation (RV)	Status
Rude	10000	319,000	0.83%	rejected
Average	20000	321.703	0.106%	Test Mesh
The End (Retained)	41000	322,046	-	Valid

The relative variation of the maximum water temperature between the medium and fine meshes is calculated as:

$$RV = \frac{322.046 - 321.703}{322.046} = 0.106\%$$

Since this value is well below the commonly accepted threshold of 0.5%, the solution can be considered independent of mesh density. The retained mesh therefore provides an adequate representation of the physical phenomena involved.

5. Conclusions and perspectives

This numerical study investigating the influence of focal length on the thermal performance of a parabolic solar cooker demonstrates that optimal thermal behavior is achieved through a slight delocalization of the absorber relative to the geometric focus. Under the simulated operating conditions of August 17 (DNI = 450 $W \cdot m^{-2}$), the results clearly indicate that controlled defocusing enhances both energy utilization and heat distribution quality within the cooking system.

Quantitatively, positioning the absorber 0.08 m below the geometric focus, corresponding to an optimal focal length of f_opt = 0.70 m, yields the best overall performance. This geometric adjustment leads to an increase of approximately 2.2 K in the maximum absorber temperature and 2.9 K in the average water temperature compared to the exact focusing configuration (f = 0.78 m). In addition, thermal uniformity across the bottom of the cooking pot is significantly improved, with a 23% reduction in temperature non-uniformity (ΔT). This reduction confirms that modifying the focal position enhances heat transfer efficiency, limits localized overheating, and ultimately improves cooking quality.

Despite these promising outcomes, the present work is subject to certain limitations, primarily related to the use of steady-state simulations and the assumption of ideal optical properties, such as constant reflectance. To consolidate and extend these conclusions, future research should focus on performing transient cooking analyses, including the evaluation of cooking times required to reach practical temperature thresholds, as well as experimental field validations. Such investigations would allow the assessment of the optimal focal configuration under real meteorological conditions and realistic optical constraints, thereby strengthening the practical relevance of the proposed optimization strategy.

Acknowledgements

Authors express sincere gratitude to the National Higher Polytechnic School of Douala Laboratory.

Financial supports

No funds, grants, or other financial support was received for conducting this study or for preparing this manuscript.

Competing Interests

The authors declare that they have no known competing financial interests or personal relationships that could have appeared to influence the work reported in this paper.

References

[1] Ahmed, S. M., Al-Amin, M. R., Ahammed, S., Ahmed, F., Saleque, A. M., & Rahman, M. A. (2020). Design, construction and testing of a parabolic solar cooker for rural households and refugee camps. *Solar Energy, 205*, 230–240. https://doi.org/10.1016/j.solener.2020.05.017

[2] Akoy, E. O., & Ahmed, A. (2015). Design, construction and performance evaluation of solar cookers. *Journal of Agricultural Science and Engineering, 1*(2), 75–82.

[3] Beheke, N. P. (2021). The effect of exposure to firewood on respiratory health and labor market participation in Cameroon. *Revue Française d'Économie, 36*, 163–195.

[4] Braun, J. E., & Mitchell, J. C. (1983). Solar geometry for fixed and tracking surfaces. *Solar Energy, 31*(5), 439–444. https://doi.org/10.1016/0038-092X(83)90064-0
[5] Coccia, G., Aquilanti, A., Tomassetti, S., Comodi, G., & Di Nicola, G. (2020). Design, realization, and testing of a portable solar box cooker coupled with erythritol-based phase change material thermal storage. *Solar Energy, 201*, 530–540. https://doi.org/10.1016/j.solener.2020.03.043
[6] Cuce, E., Cuce, P. M., & Bali, T. (2016). A comprehensive review on solar cookers. *Renewable and Sustainable Energy Reviews, 60*, 199–214. https://doi.org/10.1016/j.rser.2016.01.022
[7] Dontio, E., Guemene, N. D., Efa, F., & Simo, A. (2010). On the reliability of the Heliosat method: A comparison with experimental data. *Solar Energy, 84*, 1047–1058. https://doi.org/10.1016/j.solener.2010.03.010
[8] El-Sebaii, A. A., & Al-Ghamdi, A. A. (2012). Thermal performance of parabolic solar cookers. *Energy Conversion and Management, 65*, 647–656. https://doi.org/10.1016/j.enconman.2012.09.003
[9] Fernández-Reche, J., Sansom, C., & Martínez, A. (2019). Optical modeling of solar concentrating systems using Tonatiuh. *Solar Energy, 181*, 278–289. https://doi.org/10.1016/j.solener.2019.02.018
[10] Franco, J., Cadena, C., & Saravia, L. (2004). Multiple-use communal solar cookers. *Solar Energy, 77*(2), 217–223. https://doi.org/10.1016/j.solener.2004.04.003
[11] Harmim, A., Belhamel, M., & Bouhadda, Y. (2010). Experimental analysis of a box-type solar cooker with thermal storage. *Renewable Energy, 35*(6), 1324–1331. https://doi.org/10.1016/j.renene.2009.11.018
[12] Herez, A., Ramadan, M., & Khaled, M. (2018). Review on solar cooker systems: Economic and environmental assessment for different Lebanese scenarios. *Renewable and Sustainable Energy Reviews, 81*, 421–432. https://doi.org/10.1016/j.rser.2017.07.063
[13] International Energy Agency. (2022). *World energy outlook 2022*. IEA.
[14] Kalogirou, S. A. (2004). Solar thermal collectors and applications. *Progress in Energy and Combustion Science, 30*(3), 231–295. https://doi.org/10.1016/j.pecs.2004.02.001
[15] Khalifa, A. N., & Al-Mutawa, N. K. (1993). Thermal performance of a parabolic solar cooker. *Energy Conversion and Management, 34*(2), 203–208. https://doi.org/10.1016/0196-8904(93)90074-G
[16] Kihwele, J. E., Njau, K. N., & Mushi, A. (2020). Optimizing focal area in parabolic solar cookers for uniform heat distribution. *Solar Energy, 198*, 78–88. https://doi.org/10.1016/j.solener.2020.01.032
[17] Kurzweg, U. H., & Benson, J. D. (1982). Iso-intensity absorber configurations for parabolic concentrators. *Solar Energy, 26*(3), 195–199. https://doi.org/10.1016/0038-092X(81)90035-3
[18] Mahmut, S. B., & Saffa, B. R. (2015). Building-integrated solar thermal collectors: A review. *Renewable and Sustainable Energy Reviews, 51*, 327–346. https://doi.org/10.1016/j.rser.2015.06.009
[19] Othman, M. Y., Yatim, B., Sopian, K., & Bakar, M. N. A. (2006). Performance analysis of a solar parabolic cooker. *American Journal of Applied Sciences, 3*(9), 1947–1951.
[20] Oudjedi, S., Boubghal, A., Chaouch, W. B., Chergui, A., & Belhamri, A. (2008). Parametric design of a solar air collector intended for drying applications. *Revue des Énergies Renouvelables, SMSTS*, 255–266.
[21] Reda, I., Andreas, A., & Sengupta, M. (2014). Optical and thermal modeling of solar concentrators. *NREL Technical Report*.
[22] Schwarzer, K., & Silva, M. E. V. (2008). Characterisation and design methods of solar cookers. *Solar Energy, 82*(2), 157–163. https://doi.org/10.1016/j.solener.2007.06.002
[23] Soro, D., Modibo, S., Siaka, T., & Aka, B. (2019). Comparative cooking tests of parabolic and elliptical solar concentrators installed in greenhouse environments. *International Journal of Materials Engineering and Technology, 18*(2), 67–89.
[24] Srinivasan, M., & Kulkarni, L. V. (1978). A simple technique for fabrication of parabolic concentrators. *Solar Energy, 22*, 463–465. https://doi.org/10.1016/0038-092X(78)90059-4
[25] Telkes, M. (1959). Solar cooking ovens. *Solar Energy, 3*(1), 1–11. https://doi.org/10.1016/0038-092X(59)90002-3
[26] Zafar, H. A., Khan, M. Y., Badar, A. W., Tariq, R., & Butt, F. S. (2018). Introducing a novel design in the realm of box-type solar cookers: An experimental study. *Journal of Renewable and Sustainable Energy, 10*(4). https://doi.org/10.1063/1.5037466